LAMINOGRAPHIC RECONSTRUCTION FROM REAL-TIME RADIOGRAPHIC IMAGES

Marion D. Barker

Lockheed Missiles & Space Co.
815 E. Middlefield Rd.
Mountain View, CA 94043

INTRODUCTION

Laminography is used to separate overlying structures by focusing on various planes or surfaces in the object. This has typically been performed using film as the imaging medium. In medical laminography, also referred to as conventional tomography, the x-ray source and film are in motion during the exposure, pivoting about a plane in the object. Details within that plane are in focus in the final film exposure; in contrast, details in planes above and below the pivot plane are blurred. However, this technique requires a new exposure for each plane to be examined, and complicated mechanical arrangements are employed to pivot the x-ray source and film cassette correctly. Digital laminography, on the other hand, uses multiple digital projection images taken statically through the object tilted at discrete angles. These images are then backprojected and combined to focus on a particular depth. The advantage of digital laminography is that the same data can be used to reconstruct many different planes. Thus one can scroll through different depths in the object to determine the variation of structure with depth. In addition, the object manipulation is much simpler than the source/detector pivoting required in conventional laminography.

In this paper, we report the application of digital laminography reconstruction methods to real-time radiographic (RTR) images. Multiple digital images were acquired with the part at several orientations. Several acquisition and reconstruction methods have been investigated and their effects on the depth resolution and signal-to-noise ratio (SNR) of the reconstructed images will be discussed.

DATA ACQUISITION

The RTR projection images were acquired using a low-light level isocon camera viewing an x-ray to light conversion screen. The video signal from the isocon camera was digitized by a Recognition Concepts, Inc. Trapix 55/128 image processor. To improve the SNR of the projection images, the real-time video was digitized and integrated for 256 frames (8.5 sec). The most significant 8 bits of the integrated image were stored.

Figure 1 illustrates the geometry used in data acquisition. The object was placed on a computer controlled rotational manipulator. The three-dimensional object was radiographically projected on to the two-dimensional image plane. The unprimed coordinates (x,y,z) represent positions with respect to the object frame of reference and primed coordinates (x',y',z') represent positions with respect to the lab frame of reference (unrotated axes). The projection from lab coordinates to image coordinates (u,v) is

$$u = D\,x' / (d - z')$$
$$v = D\,y' / (d - z') \qquad (1)$$

where D is the source to screen distance and d is the source to object (center of rotation) distance.

The mapping from body coordinates to lab coordinates is obtained by using the appropriate rotation and displacement matrices $\underline{M}$ and $\underline{D}$ which are dependent on the number and order of rotations and displacements and thus must be calculated for each particular manipulator configuration. The data presented is this paper were all acquired with a single rotation, θ, about the y axis with no displacement. By no displacement, we mean that the vector from the x-ray focal spot through the center of axis of rotation is perpendicular to the image plane and intersects the origin of the image coordinate system. In addition, the direction cosines of the u axis and x axis are parallel as are those of the v and y axes. The matrix $\underline{M}$ is then a simple rotation matrix while $\underline{D}$ is the null matrix. For any given θ, the mapping from (x,y,z) to (u,v) is

$$u = \frac{D(x\cos\theta + z\sin\theta)}{d + x\sin\theta - z\cos\theta},$$
$$v = \frac{Dy}{d + x\sin\theta - z\cos\theta}. \qquad (2)$$

The camera tube position within the yoke was carefully adjusted so the pixel coordinate axes (iu,iv) correspond to the (u,v) axes.

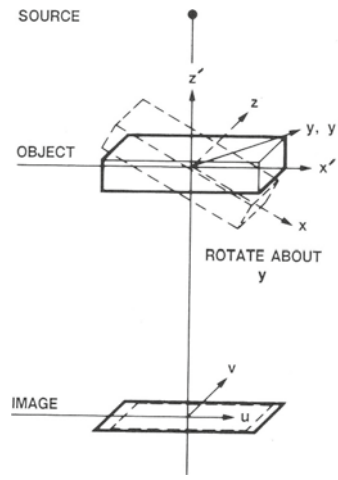

Fig. 1. Geometry used in data acquisition of projection images.

IMAGE RECONSTRUCTION

For a given value of z, or depth, in the object, Eq. (2) can be inverted, i.e., the images can be backprojected to the selected plane, z. The basic reconstruction idea used in laminography is that if a feature in the image is actually at that depth, then the calculated (x,y) coordinates will be the same for all object orientations. However, if a feature in the image is at a different depth, then the (x,y) location for that feature will be different depending on the object orientation. If the backprojected images are averaged, then features actually at the depth z will be seen at the correct location with full intensity while features at a different depth will be spatially blurred and with lower intensity.

The backprojection may be made to any surface z = f(x,y). However, this increases the complexity of the reconstruction and thus slows down the calculation. For this paper, all reconstructions were performed for a plane of constant z.

The projection images used for reconstruction are stored in the image processor memory for faster reconstruction times. Since there are 16 memory planes of 512 x 512 pixels x 8 bits, and one memory is required for the reconstructed image, we imposed a practical limit of 15 projection images for laminographic reconstruction. As will be shown in the EXPERIMENTAL RESULTS section, good reconstructions can be obtained with as few as 8 images.

The backprojection for a particular depth z was calculated by stepping through the 512 x 512 output image pixel coordinates (ix,iy), calculating the corresponding (x,y) and then (u,v) coordinates, converting these to pixel locations in the projection image and inserting the pixel intensity of the projection image into the backprojected image. The (x,y) coordinates were calculated from the (ix,iy) coordinates using the same magnification and aspect ratio as the projection images. These scale factors can be adjusted to utilize a different fraction of the 512 x 512 pixels available, if desired.

Three reconstruction methods were tested: (1) standard, (2) extreme value and (3) iterative. We define $P_i(x,y)$ as the ith image backprojected to the selected z plane and T(x,y) as the reconstructed image. The standard method uses a straight average of the N backprojected images:

$$T(x,y) = \frac{1}{N} \sum_{i=1}^{N} P_i(x,y) \tag{3}$$

The extreme value method of Haaker [1] selects the value from the N backprojected images with minimum value, i.e.,

$$T(x,y) = \underset{i=1}{\overset{N}{\text{MIN}}} \left(P_i(x,y)\right) \tag{4}$$

This is particularly useful in separating high contrast features from the background in negative video images. However, since only one value is selected from the N projections, the SNR is degraded somewhat.

To improve the SNR of the reconstruction, Kruger [2] modified the extreme value method and developed the iterative method. The superscript refers to the iteration number where an iteration of 0 is the same as the standard method and an infinite number of iterations is the same as the extreme value method.

$$P_i^j(x,y) = \min_{i=1}^{N} [T^{j-1}(x,y),\ P_i^{j-1}(x,y)]$$

$$T^j(x,y) = \frac{1}{N} \sum_{i=1}^{N} P_i^j(x,y) \qquad (5)$$

In programming the iterative method, a compromise between space and speed resulted in a limit of 8 projection images for the iterative method for this paper. Typical reconstruction times for a 512 x 512 output image reconstructed from 8 projection images are 4 minutes for the standard and extreme methods and 11 and 14 minutes for 2 and 4 iterations respectively. The reconstruction times increase with more projection images.

For both extreme value and iterative reconstructions, care must be taken to properly normalize the projection images. Since the minimum value of the individual images is enhanced, it is important that the background pixel level be the same in all projections. The images in this paper were all taken of rectangular objects. As the angle differs from 0 degrees, the path length through the material increases, lowering the transmitted x-ray flux and thus increasing the measured pixel value (inverse video). For low contrast features, the change in intensity due to this effect can be greater than that due to the features. In this worst case, extreme value reconstruction would always select values from the 0 degree backprojection because the overall pixel values are lower for this image. To correct this tendency, the projection images were normalized using a linear look up table so that the mean value of the background signal in each normalized images is equal to the average mean value of the background signals in the original projection images. For the objects of arbitrary shape, a more general normalization scheme would need to be developed.

EXPERIMENTAL RESULTS

Projection data were acquired using two phantoms: one to test depth separation and one to test the sensitivity of the reconstruction methods. The results of these tests will be discussed in the next two subsections.

Depth Separation

The depth separation phantom is shown schematically in Fig. 2a. It is composed of 5 layers mounted on 1/4" lucite plates. The plates are fastened together with nylon threaded rod and are separated by 1/32" nylon washers. The features are made from 0.03" Al wire in straight lines and shaped into representations of the letters A, B, C, D, and E on adjacent layers, 1/32" nylon washers, and a razor blade located on the "C" layer. Eleven projection images were acquired for θ = +/-40, +/-35, +/-28, +/-20, +/-10 and 0 degrees. All images were acquired with a source to screen distance of 1400 mm, geometric magnification of 1.2, x-ray source parameters of 70 kV and 2mA, and 256 frames (8.5 sec) of integration. Figure 2b is the 0 degree radiographic projection image of the phantom.

All 11 images were used for the standard and extreme value reconstructions. A subset of 8 images was selected for the iterative method with θ = -40, -28, -20, 0, 10, 20, 35, and 40 degrees. Figure 3 shows reconstructions of the "C" layer for all three methods. The improvement in depth separation of the extreme value and iterative methods over the standard method can be clearly seen. Figure 4 shows reconstructions of the 5 separate layers using the extreme value method.

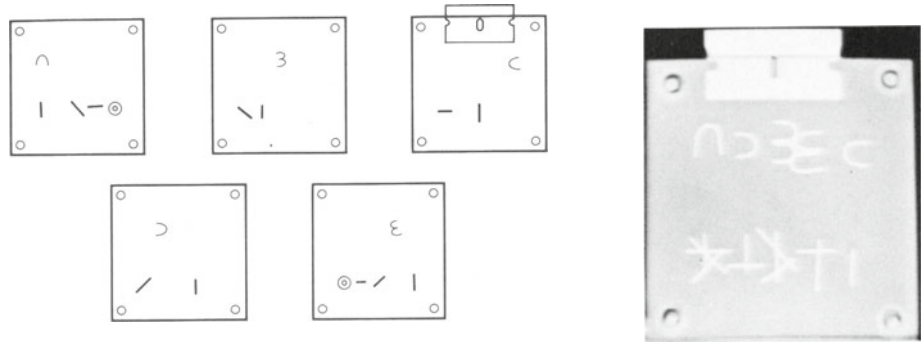

a b

Fig 2. (a) Layout of depth separation phantom. The lines indicate Al wire, the rings are nylon washers placed on 1/4" lucite plate. The plates are fastened together with nylon rod. (b) Projection radiograph of phatom acquired at θ= 0 degrees.

Signal-to-Noise Ratio

The sensitivity phantom is shown schematically in Fig. 5a. It is composed of a 1" thick plate of Al with features on the front and back surfaces. On the front is a 0.005" tungsten shim, a 4% ASTM penetrameter and a 1/32" Al shim. On the back is the letter M shaped out of solder and a 3% ASTM penetrameter. Fifteen projection images were acquired for = +/-40, +/-35, +/-28, +/-20, +/15, +/-10, +/-5, and 0 degrees. All images were acquired with a source to screen distance of 1400 mm, geometric magnification of 1.2, x-ray source parameters of 160 kV and 3mA, and 256 frames (8.5 sec) of integration. Figure 5b is the 0 degree projection image of the phantom.

A subset of 8 images was selected for the iterative method with θ = -40, -28, -10, 0, 5, 10, 28, and 40 degrees. Figure 6 shows images of the front and back surfaces using iterative reconstruction with 2 iterations.

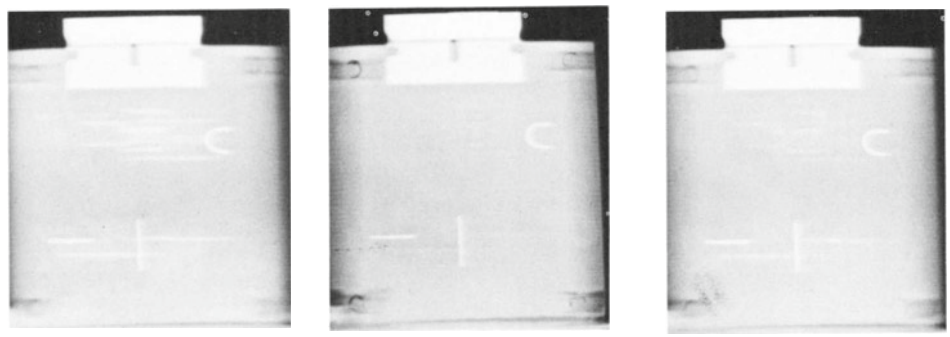

a b c

Fig. 3 Reconstruction of phantom shown in Fig. 2 at a depth of -6.0 mm using (a) standard method, (b) extreme value method, and (c) iterative method with 2 iterations.

a b c

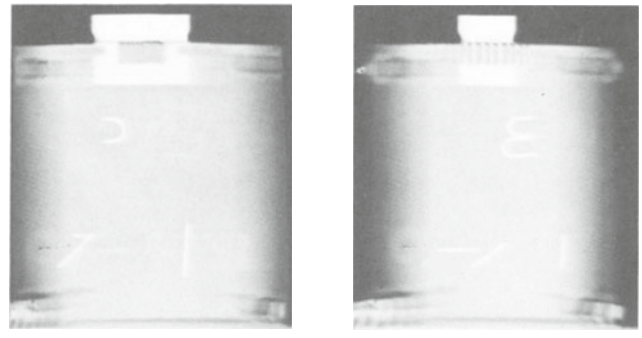

d e

Fig. 4 Extreme value reconstruction of phantom shown in Fig. 2 at depths of (a) -19.5 mm, (b) -12.5 mm, (c) -6.0 mm, (d) 0.5 mm, (e) 7.5 mm.

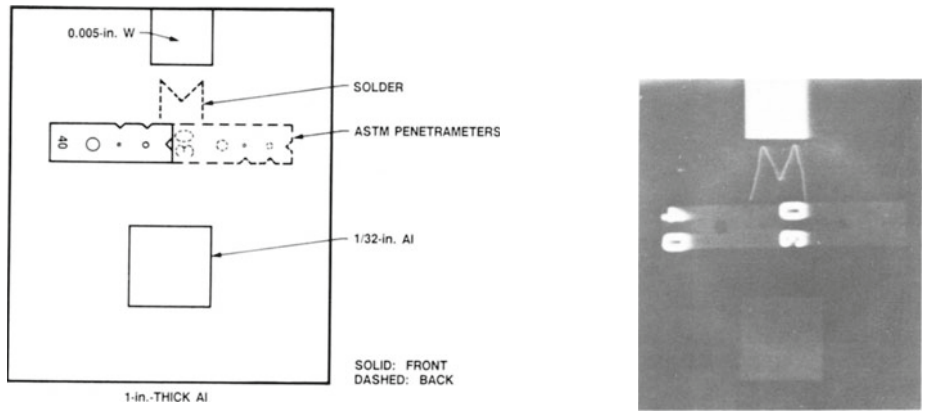

a b

Fig. 5 (a) Layout of sensitivity phantom. The solid lines indicate features on front of 1" thick A1 plate; dashed lines indicate features on back of plate. (b) Projection radiograph of sensitivity phantom acquired at $\theta = 0$ degrees.

To quantitatively compare the sensitivity of different reconstruction methods and input angle sets, the SNR was measured for the 1/32" Al shim. Since RTR images are not uniform, the shading correction method of Barker [3] was used. A quadratic from was fitted to the region of the shim and the background region around the shim. The two regions were simultaneously fitted to the same function with the exception of the constant term. The difference in the constant term is then the signal due to the presence of the shim and the noise is the square root of the chi-squared per degree of freedom. The SNR is plotted in Figs. 7 and 8.

Figure 7 shows the SNR as a function of reconstruction depth for iterative reconstruction using 2 iterations with the same angle set as Fig. 6. The shim is actually located at -12 mm and the peak in the SNR occurs around -13 mm. We are not sure what causes the discrepancy between best focus of the shim and best SNR of the shim. There was a ring artefact in the camera tube, not removed using the shading correction described above, which may have caused this discrepancy. This will certainly be investigated further as one would expect the peak in focus and SNR to occur at the same depth. The peak in the SNR occurred consistently at -13 mm for standard, extreme value, and iterative reconstruction methods and with several different angle sets.

Figure 8 shows the effect of different reconstruction methods, number of projection images and angular range on the SNR at a depth of -12 mm. Figure 8a shows the effect of reconstruction type on the same angle set used in Fig. 6. The standard method yields the highest SNR, with the SNR decreasing with the number of iterations and being the lowest for the extreme value method. The SNR of the 1/32" shim of the 0 degree projection image was 2.5. Figure 8b shows the effect of the number of images and angular range on the SNR. The angle sets used were (from left to right), (1) all images, (2) same as Fig. 7, (3) Θ= -20, -15, -10, -5, 0, 10, 15,and 20 degrees, (4) same as (1), and (5) same as (2). For the standard method, the SNR increases with the number of images for a fixed angular range and with increased angular range for a fixed number of images. The extreme value method indicates that the SNR actually decreased in going from 8 to 15 images with the same angular range. We investigated further and found the SNR to increase as the number of projections was increased from 4 to 8 and then to decrease as the number of projections was increased to 15. However, the variation in SNR for these different number of projections is less than 10% and is probably due to a systematic effect. If the results were solely governed by Poisson statistics, the SNR would increase as a function of the number images.

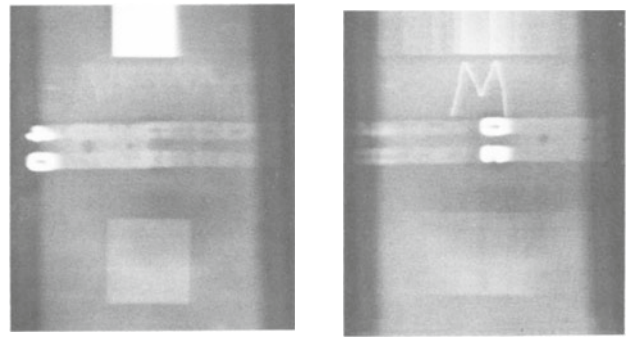

a b

Fig. 6 Iterative reconstruction with 2 iterations of phantom shown in Fig. 5 at a depth of (a) -12.0 mm (front of plate) and (b) 14.5 mm (back of plate.)

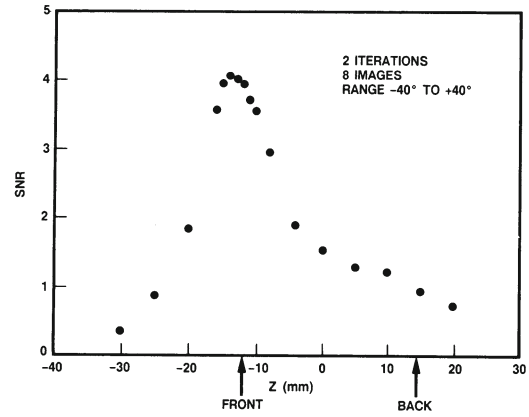

Fig. 7. Signal-to-noise ratio of 1/32" Al shim in images reconstructed with 2 iterations as a function of depth.

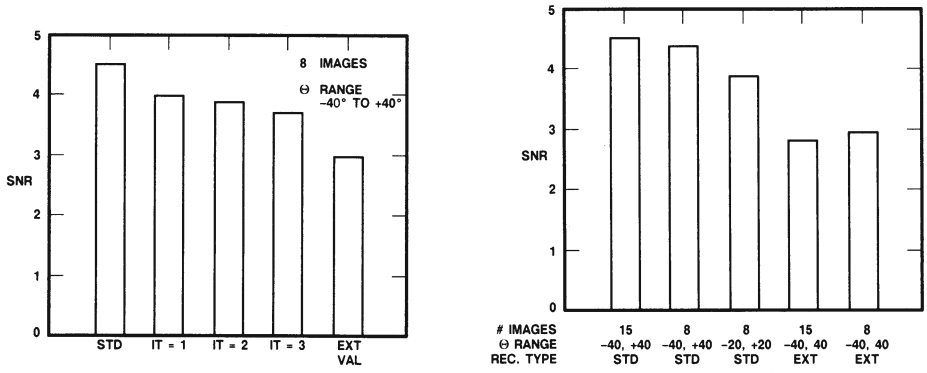

a b

Fig. 8. Signal-to-noise ratio of 1/32" Al shim in reconstructed images at depth of -12.0 mm for (a) different reconstruction methods and (b) different angle ranges and number of projection images.

CONCLUSIONS

We have shown that good laminographic reconstructions can be obtained from real-time radiographic images. This capability can be added to existing RTR systems with the addition of simple software. Three reconstruction techniques have been presented. The standard method yields the best signal-to-noise but the worst depth separation; the extreme value method yields the best depth separation with a slight decrease in signal-to-noise; and the iterative method is a compromise between the two. Both the extreme value and iterative methods require care in properly normalizing the projection images.

REFERENCES

1. P. Haaker, et al, Med. Phys. 12, 431 (1985)
2. R. A. Kruger, et al, Med. Phys. 14, 940 (1987)
3. M. D. Barker, et al, in Review of Progres in Quantitative NDE, ed by D. O. Thompson, D. E. Chimenti, (Plenum Press, New York, 1988) Vol. 7A pp. 333-341